

ARTICLE OPEN



Soil moisture revamps the temperature extremes in a warming climate over India

Naresh G. Ganeshi^{1,2}, Milind Mujumdar¹✉, Yuhei Takaya³, Mangesh M. Goswami¹, Bhupendra Bahadur Singh¹, R Krishnan¹ and Toru Terao⁴

Soil moisture (SM) plays a crucial role in altering climate extremes through complex land-atmosphere feedback processes. In the present study, we investigated the impact of SM perturbations on temperature extremes (ExT) over India for the historical period (1951–2010) and future climate projection (2051–2100) under 4 K warming scenario. We note that more than 70% area of the Indian landmass has experienced significant changes in characteristics of ExT due to SM perturbations. In particular, we see larger impact of SM perturbations on ExT over the north-central India (NCI), which is a hotspot of strong SM-temperature coupling. Over NCI, a 20% departure in SM significantly revamps frequency, duration and intensity of ExT by 2–5 events/year, 1–2 days/event and 0.5–2.1 °C, respectively, through modulating surface energy partitioning, evapotranspiration and SM memory. Importantly, the impact of SM perturbations on frequency and duration of ExT events becomes less prominent with intensification of global warming.

npj Climate and Atmospheric Science (2023)6:12; <https://doi.org/10.1038/s41612-023-00334-1>

INTRODUCTION

Major land regions of the world have been exhibiting severe rise in temperature extremes (ExT) during the recent few decades¹. The Indian subcontinent has been highlighted as one of the hotspots for increased characteristics of ExT^{2,3}. Recent studies have projected that outbreak of high-intensity ExT is likely to become more common over India at the end of the 21st century^{4–8}. The Indian region generally experienced the extreme heat conditions during the pre-monsoon months of April–May–June^{9,10}, which may elongate into the summer monsoon season as well, due to prolonged deficiency of the monsoon rainfall^{11–13}. Furthermore, increase in ExT exerts serious impact on the ecosystem, human health, agriculture and economy^{14,15}.

Understanding long-term changes in ExT over India in past and future climate has been an important topic of research^{12,14,15}. Observations indicate that occurrence of ExT over India is linked to large-scale atmospheric circulation anomalies and regional-scale land-atmosphere feedback processes arising from soil moisture (SM) variations^{16–19}. In particular, SM revamps the ExT by modulating the surface energy partitioning and evapotranspiration (ET)^{13,20,21}. As a crucial component of land-atmosphere coupling processes, SM also acts as temporal storage of atmospheric anomalies^{22–25}. Additionally, the long-term persisting nature (memory) of SM has potential to induce a pronounced impact on near-surface temperature and precipitation (PR) variability^{13,26}. Therefore, it is very important to understand the regional-scale SM variability using observational datasets and model simulations to get better insight into land-atmosphere feedback processes associated with extreme temperature conditions^{13,20,27,28}.

The influence of SM on ExT can be determined using the observational data products^{13,17,29} as well as state-of-the-art climate model sensitivity experiments initialized by perturbing SM^{30,31}. In review of the SM sensitivity experiments over the Indian landmass, researchers mostly explored SM-PR feedback

mechanism using the model simulations^{32–34}. However, impact of SM perturbations on ExT over India is still unclear. Therefore, this study aims to investigate the impact of SM perturbations on ExT by using the Meteorological Research Institute (MRI) high-resolution (~60 km) atmospheric general circulation model (i.e. MRI-AGCM3.2³⁵) simulations (refer to sub-section Model and experimental setups for more details) for the historical period (1951–2010) and future projection (2051–2100).

RESULTS

Model evaluation

In this section, we will first evaluate the simulation of some of the key surface hydro-meteorological variables (PR, SM, ET, and maximum temperature: T_{\max}) over the Indian region from the historical (HIST) experiment with respect to observed datasets. Time-mean (1951–2010) spatial maps of PR, T_{\max} , SM and ET are shown in Fig. 1 from the HIST experiment (1st row) and observational data products (2nd row). While the model simulation broadly captures the spatial pattern of annual mean PR, SM and ET, such as the relatively higher values over the west coast, north-central and north-eastern parts of India and lower values over the north-west India, there are also noteworthy differences between the simulated and observed hydro-meteorological variables. For example, it can be seen that the simulation indicates drier PR, lower ET and drier SM over the Indo-Gangetic plains as compared to observations. We also note that the simulated annual mean T_{\max} is underestimated over much of the Indian region as compared to the observed data.

Model biases at regional and sub-regional scales basically arise due to differences in statistical properties of the simulated and observed climatic variables (e.g., PR and T_{\max}), which need to be taken into account for model evaluations (see Soriano et al.³⁶). Keeping this in view, we have applied the bias correction method suggested by Soriano et al.³⁶ to the simulated hydro-

¹Centre for Climate Change Research, Indian Institute of Tropical Meteorology, Ministry of Earth Sciences, Pune 411008, India. ²Savitribai Phule Pune University, Pune 411007, India. ³Meteorological Research Institute, Ibaraki 305-0052, Japan. ⁴Faculty of Education, Kagawa University, Kagawa 760-8522, Japan. ✉email: mujum@tropmet.res.in

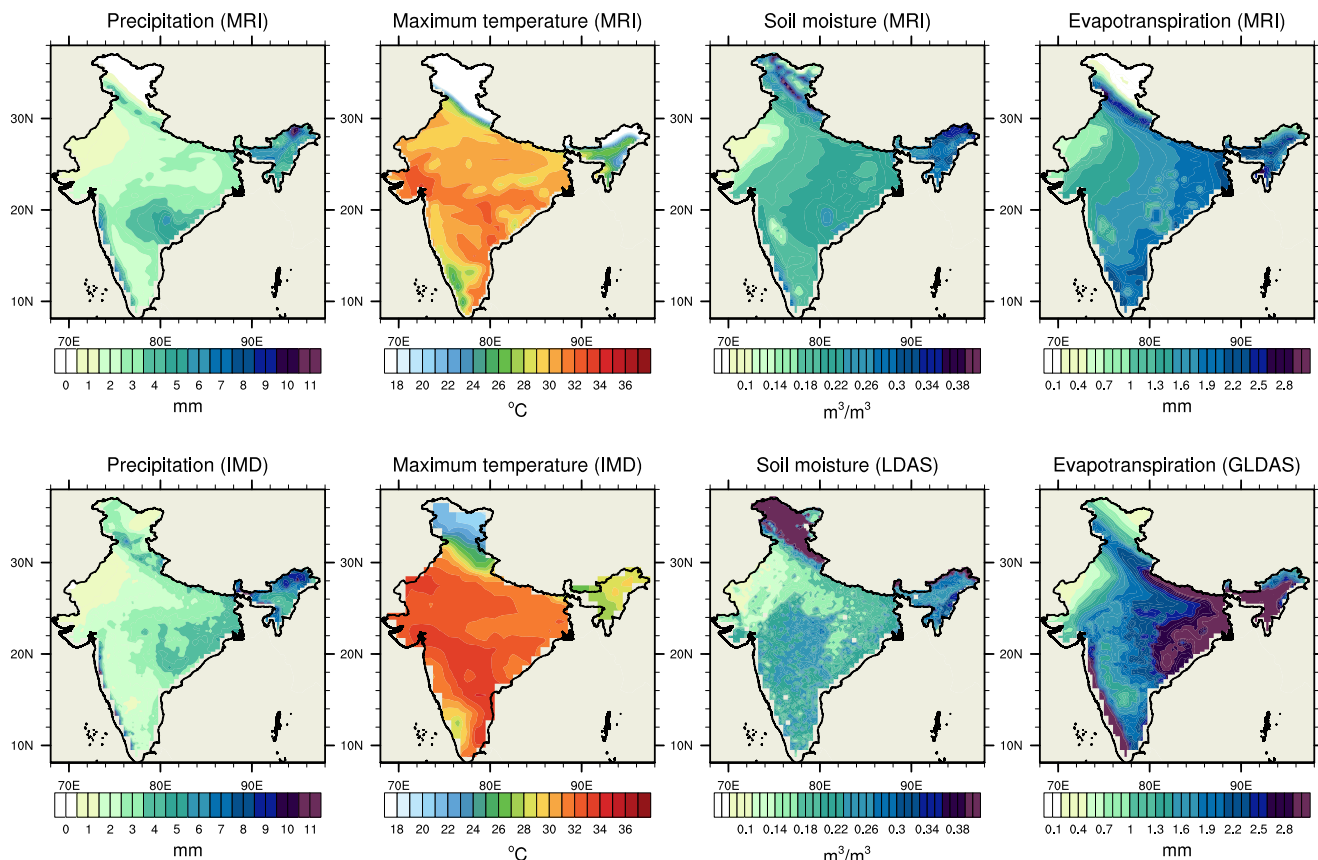


Fig. 1 Climatological features of hydro-meteorological variables for period 1951–2010. Time-mean spatial maps of annual mean precipitation (1st column), maximum temperature (2nd column), soil moisture (3rd column) and evapotranspiration (4th column) from the model simulations (1st row) and other data products (2nd row) for the historical period (1951–2010).

meteorological variables. Fig. 2 shows the Taylor diagram³⁷ analysis of PR, SM, T_{\max} and ET averaged over the Indian region based on the bias-corrected model outputs (left panel), and raw (uncorrected) model simulations (right panel). The results of the Taylor diagram analysis suggest that the bias-corrected PR, SM, T_{\max} and ET over the Indian landmass simulated by the model compares well with observations w.r.t correlation, standard deviation, and root mean square error. It can be seen that the annual-mean bias-corrected hydro-meteorological variables show high correlations in the range of (0.75–0.91), standard deviations close to the observations in the range of (0.94–1.1), and reduced root mean square deviation in the range of (0.45–0.65). The improved Taylor statistics of the hydrological variables provides motivation to examine the role of SM on ExT over the Indian region.

Soil moisture-temperature (SM-T) coupling over the Indian region

SM has a dominant influence on temperature variability and, as a result, on ExT over the regions of strong land-atmosphere coupling²⁰. Here, we aim to understand the SM-T coupling for historical period (1951–2010) and future projection (2051–2100) using the linear regression method as suggested by Dirmeyer³⁸ (see Methods). Additionally, diagnosis of coupling strength is extended on the entire annual cycle to explore the role of SM on annual extremes beyond pre-monsoon months. Fig. 3 indicates spatial distribution of SM-T coupling strength (Ω) across the Indian region. Result shows that hotspot of strong SM-T coupling is located over the north-central India (NCI). Stronger coupling over the NCI reveals significant control of SM on near-surface temperature variations. Spatial pattern of SM-T coupling nearly coincides with the coupling hotspot highlighted in recent study

by Ganeshi et al.¹³ over India. The coupling strength estimated from Dirmeyer³⁸ also cross validated using the method by Miralles et al.²⁷. It is noted from Supplementary Fig. 4, 5, and Fig. 3a that spatial coupling patterns based on the metric π and Ω are consistent with each other.

SM-T coupling over the land is mainly influenced by the combined effect of water availability at the top surface and radiational energy²⁰. Weaker coupling over the wet and the dry regions (Fig. 3) is due to the limited available radiational energy and less evapotranspiration variability, respectively. On the contrary, imposing dominant control on evapotranspiration, moderate SM regimes of NCI indicate to have larger impact on near-surface temperature variability^{13,20}. Investigation of SM-T coupling is further extended for the FUT experiment (4 K warming scenario), which shows similar spatial distribution of SM-T coupling strength over India as that of HIST experiment. From Fig. 3b, it is to be noted that the area of strong SM-T coupling is likely to expand under the FUT 4 K warming experiment. The expansion or shrinking of strong SM-T coupling regions can be a significant aspect of climate change⁷.

Long-term mean of temperature extremes

Fig. 4 shows spatial distribution of long-term mean extreme temperature frequency (ExTF), duration (ExTD), and intensity (ExTI) over the Indian region from the HIST and FUT experiments. Estimates of ExTF, ExTD and ExTI are carried out using bias-corrected T_{\max} simulations from MRI-AGCM3.2. Spatial maps of these extremes for the HIST experiment indicate at least 4 events per year over the Indian landmass with an average duration of ~5 to 6 days per event and maximum intensity of about 47 °C is seen over the central India (Fig. 4). It is noted that the pattern correlation

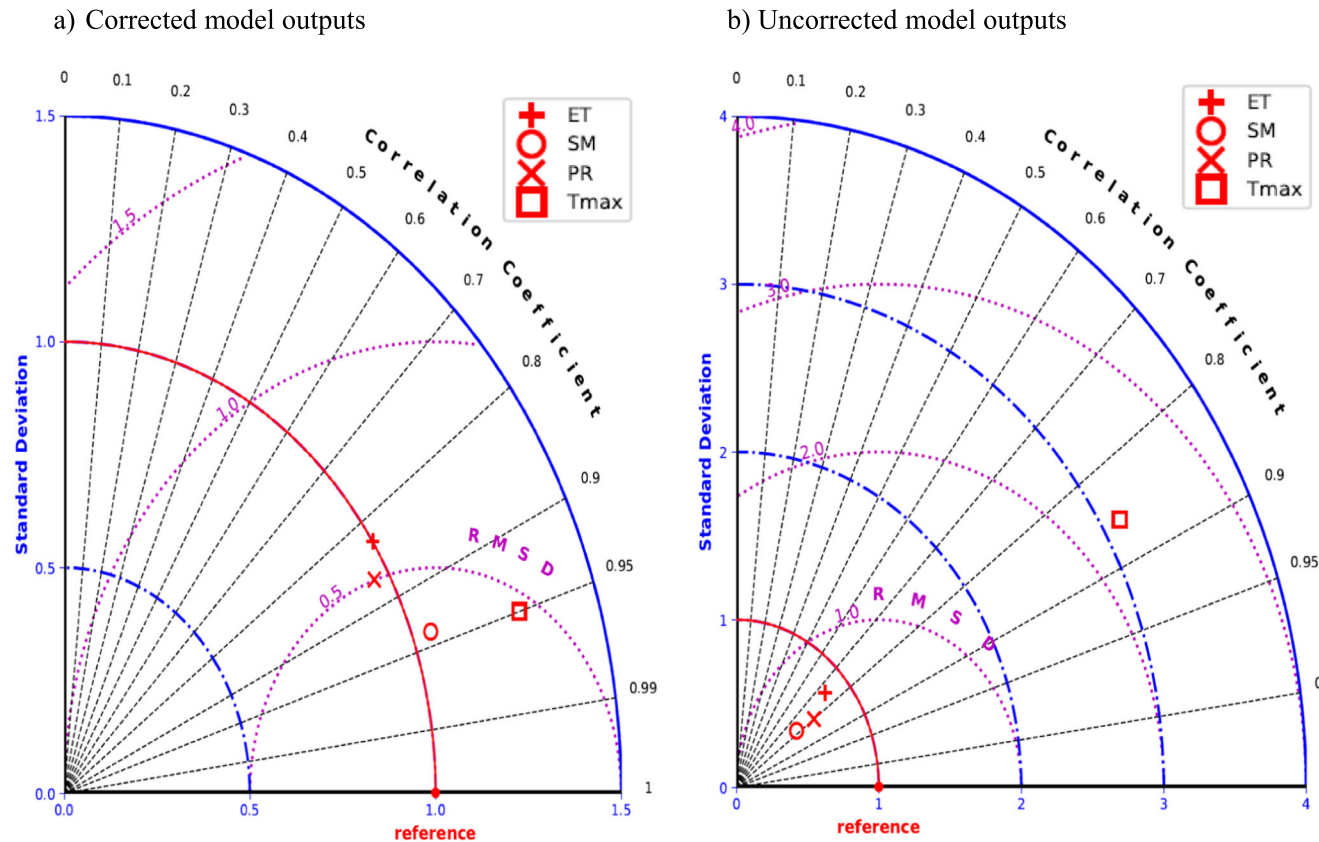


Fig. 2 Comparison of corrected and uncorrected model outputs using Taylor statistics. Taylor diagram showing statistics of annual-mean PR, T_{\max} , SM, and ET averaged over the Indian region based on the (a) corrected model outputs and (b) uncorrected model outputs. Taylor statistics represented using the correlation coefficient (black line), standard deviation (blue line), and root mean square deviation (purple line) with respect to observed data products.

of extreme temperature characteristics (ExTF, ExTD and ExTI) between HIST and IMD observations exceeds 0.4 (significant at 95% confidence) over the Indian region. Future changes in extremes for the period 2051–2100 are also evaluated here under the 4 K warming scenario. Future simulation suggests alarming increase in extreme temperature characteristics almost over the entire (covering ~100% area) Indian landmass (Fig. 4). On an average, the FUT experiment suggests an increase of ~9 ExT events per year with an average increase of ExTD about 5–6 ExT days per event and ExTI about 3 °C ExTI w.r.t the HIST experiment. The severity of ExT from the FUT experiment also indicates significant impact of climate change on ExT under 4 K warming scenario.

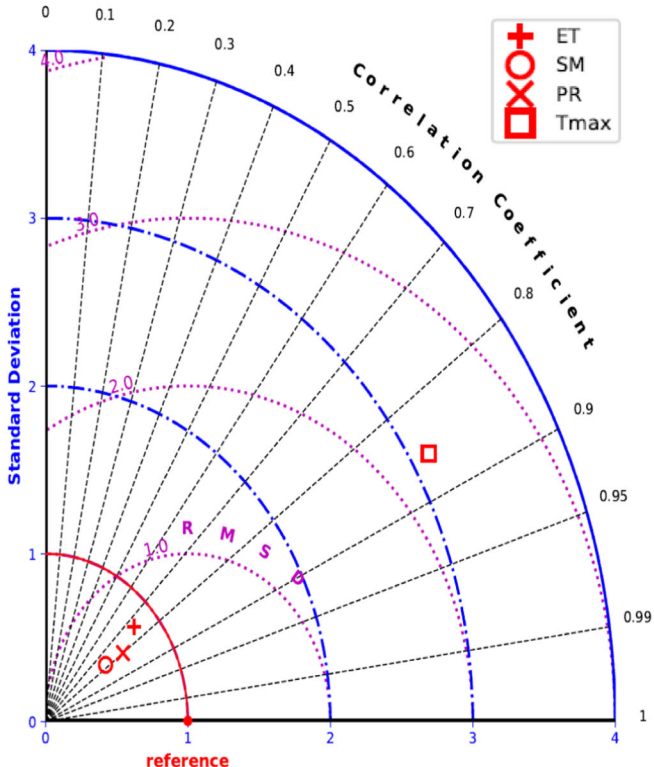
We further carry out analysis of extremes over the strong SM-T coupling region of the NCI. Area-averaged time series over the NCI is used to evaluate long-term changes in ExTD, ExTF and ExTI for the HIST and the FUT experiments. Over the NCI, the HIST simulation indicates occurrence of 4–5 ExT events per year, with an average intensity greater than 46 °C and duration of 5–6 days per event (Supplementary Fig. 9). Furthermore, the FUT experiment indicates severe rise in ExT characteristics over the hotspot of strong SM-T coupling (NCI) under 4 K warming scenario. Our findings show that high intensity ($ExTI > 50$ °C) ExT events are likely to occur after every 25–30 days in future (4 K warming scenario) over India, which can prevail at least for 10 to 12 days (Supplementary Fig. 9).

Impact of soil moisture perturbations on temperature extremes

In the present study, we have explored the impact of SM on ExT for the historical period (1951–2010) and future projection

N.G. Ganeshi et al.

b) Uncorrected model outputs



(2051–2100) using wet and dry SM sensitivity experiments (listed in Supplementary Table 1). Columns second and third in Fig. 5 shows mean change in ExTF, ExTD and ExTI from the HIST-20 (decrease of SM by 20% w.r.t HIST) and HIST + 20 (decrease of SM by 20% w.r.t HIST) experiments w.r.t the HIST simulation, respectively. On an average, drier SM conditions (HIST-20) increase the ExTF by 4–5 events per year, ExTD by 1–2 days per event, and long-term mean ExTI at least by 0.6 °C (Fig. 5). In contrast, wet SM conditions (HIST + 20) tend to reduce ExTF, ExTD and ExTI by 1–2 events per year, 2–3 days per event and ~0.5 °C (long-term mean), respectively (Fig. 5). Future climate sensitivity experiments demonstrate similar results to historical simulations, albeit with a smaller impact of soil moisture over the Indian region. The FUT-20 simulation intensifies ExT by 1–2 events per year, 0–1 days per event and long-term mean ExTI by ~1 °C than that of the FUT experiment (Fig. 6). Whereas results from the FUT + 20 experiment indicate reduction of ExTF by 3–4 events per year, ExTD by 3–4 days per event, and long-term mean ExTI by ~2 °C (Fig. 6). A comparison between the control (HIST and FUT) and the sensitivity experiments (HIST-20, HIST + 20, FUT-20 and FUT + 20) indicate that almost 70% or more area of the Indian region has experienced significant change in the ExT characteristics.

The main aim of this study is to understand the role of SM on ExT over the hotspot of strong SM-T coupling. We noted an increase of ~5 ExT events per year over the NCI from the HIST-20 experiment, with average increase in ExTD of 1.8 days per event and ExTI ~ 0.71 °C w.r.t the HIST experiment (Fig. 7 & Supplementary Fig. 9). Whereas wet simulation (HIST + 20) reduces ExTF by ~3 events per year, ExTD by ~1 day per event, and long-term mean ExTI ~1.88 °C w.r.t the HIST experiment. The FUT-20 experiment shows an increase of ExTF by ~2.2 events per

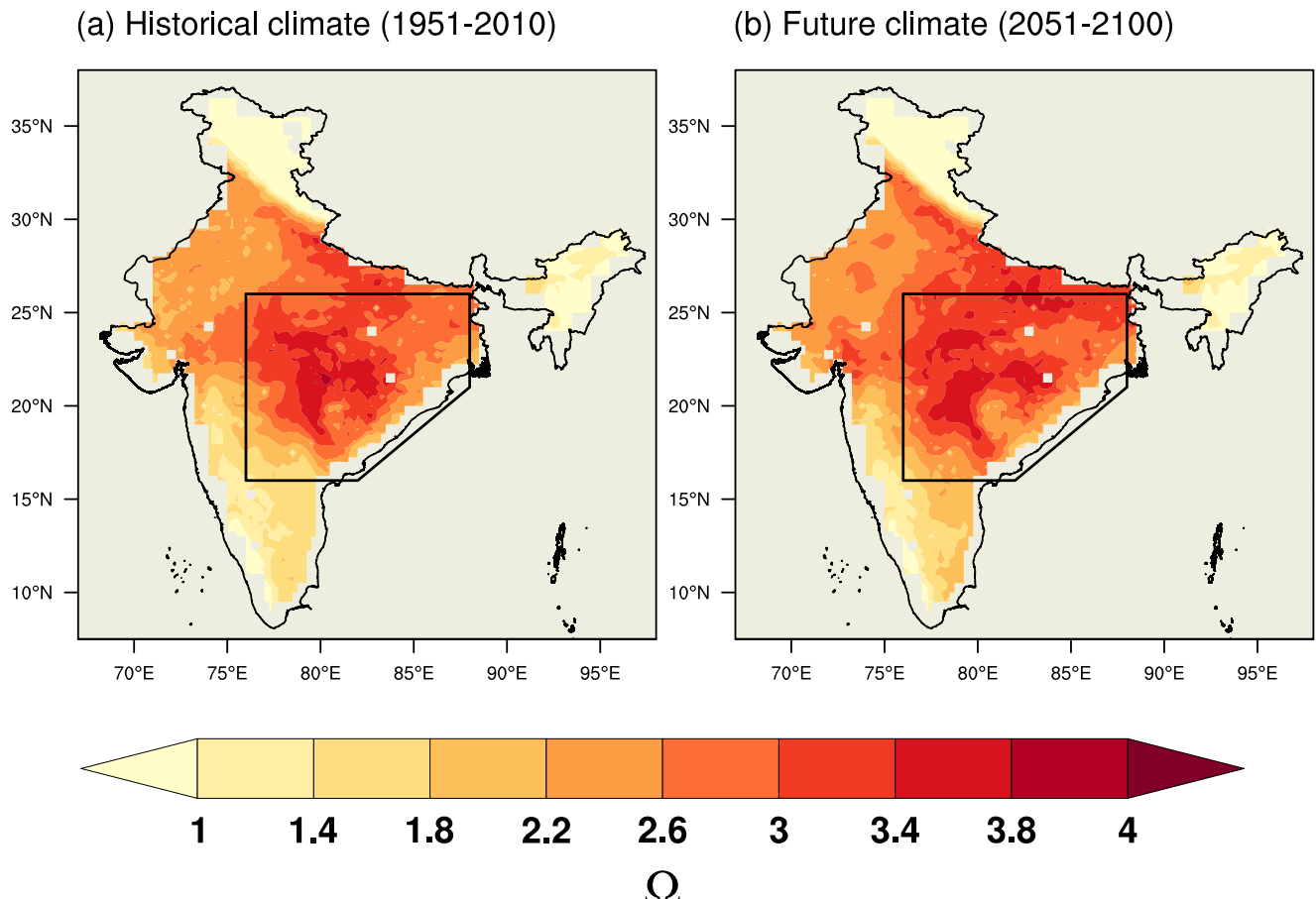


Fig. 3 Soil moisture-temperature coupling. Spatial maps of soil moisture-temperature coupling over the Indian region estimated using the method by Dirmeyer³⁸ for the (a) HIST and (b) FUT experiments. The area shown in the polygon over north-central India (NCI) is highlighted as the region of strong soil moisture-temperature coupling over India (75°E-87°E, 16°N-26°N, land only).

year, ExTD by ~ 1.55 days per event, and long-term mean intensity ~ 0.93 °C under dry SM conditions w.r.t the FUT experiment. While, we noted significant decrease in ExT characteristics (decrease of ExTF ~ 3.3 events per year, ExTD by 2 days per event and long-term mean ExTI ~ 2.02 °C) over the NCI in the FUT + 20 experiment w.r.t the FUT experiment. The sensitivity experiments reveal the significant impact of SM on ExT characteristics over the Indian region. Moreover, the dominant influence of SM on ExT can be found over the hotspot of strong SM-T coupling. Similar results are also seen from the analysis of area-averaged time series of ExTF, ExTD and ExTI over the NCI (Supplementary Fig. 9).

Analysis of ExT is also carried out using the Generalized Extreme Value (GEV) theory and probability distribution approach over the NCI. The yearly block maxima approach is applied to the non-stationary GEV model fit of ExTI index, considering SM as a covariate. Further, the influence of SM on extremes is quantified using difference between 50-year return values of block maxima as obtained from dry and wet SM sensitivity experiments. Fig. 8 shows the return level plot of yearly block maxima obtained from non-stationary GEV model fit. We noted a higher return level values of yearly T_{\max} from the dry SM perturbations (red colour curve) than the wet SM perturbations (blue colour curve). For the historical period (1951–2010), difference between 50-year return values of dry and wet SM simulations is nearly ~ 1.25 °C. In other words, a 20% decrease of SM over the NCI leads to increase the yearly maximum temperature with absolute values reaching upto 48.75 °C once in 50 years. On the other hand, for wet simulation (HIST + 20), the yearly maximum temperature remains below 47.63 °C once in 50-year. Furthermore, the FUT-20 (FUT + 20)

shows an intensification (reduction) of yearly maximum 50-year return level of temperature upto (below) 53.52 °C (50.94 °C). To strengthen the analysis of ExT, the influence of SM on extremes over NCI is discussed (see supplementary material) here using the PDFs of yearly block maxima (T_{\max}) (Fig. 9) for the control (HIST and FUT) and the sensitivity experiments (HIST-20, HIST + 20, FUT-20 and FUT + 20). It is to be noted that the results of the present paper are based on a single model simulation, therefore the impact of SM on ExT may vary in the other models depending on the representation of land-atmosphere coupling strength. In summary, analysis of sensitivity experiments reveal the crucial role of SM on ExT over the region of strong SM-T coupling. The processes illustrating the influence of SM on extremes through land-atmosphere coupling are discussed in the following subsection using the sensitivity experiments.

Response of land-atmosphere interactions to SM perturbations

In this section, we have investigated the impact of SM perturbations on land-atmosphere feedback processes (i.e. sensible heat flux: SHF, latent heat flux: LHF, ET, SM, T_{\max} & soil moisture memory: SMM) over the Indian region by using HIST, HIST-20 and HIST + 20 experiments. Columns first and second in Fig. 10 shows mean change in SM, T_{\max} , SHF, LHF, ET, & SMM from the HIST-20 and HIST + 20 experiments w.r.t the HIST simulation, respectively. ET is one of the important factors in land-atmosphere coupling processes, which is mainly controlled by SM and energy availability at land surface³⁰. Fig. 10 indicate that the regions where SM conditions are found to be wetter or drier have less

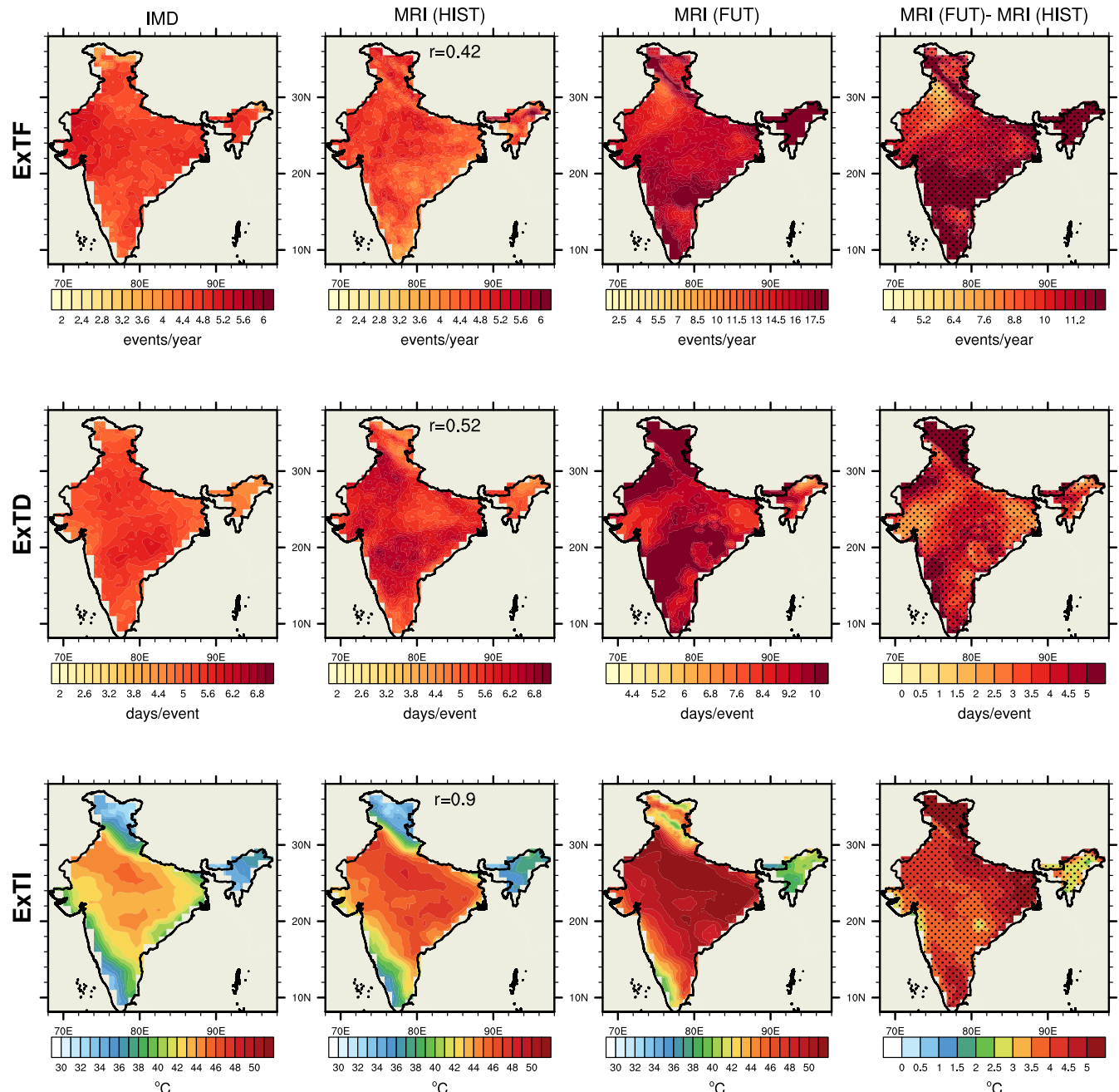


Fig. 4 Temperature extremes over the Indian region. Time-mean spatial maps of extreme temperature frequency (ExTF: 1st row), duration (ExTD: 2nd row) and intensity (ExTI: 3rd row) from the IMD observations (1st column), HIST experiment (2nd column), FUT experiment (3rd column), and difference between the FUT and HIST experiment (4th column). The pattern correlation coefficient (r) between extreme temperature indices from MRI outputs and IMD observations are given in Figures of 2nd column. Stippling in Figures indicate the regions where difference between the FUT and HIST experiments is significant at 95% confidence level.

impact on ET variability. These regions are mainly located over the north-west, north and north-east parts of India. On the other hand, maximum sensitivity of ET can be observed over moderate SM regimes, where enough SM and radiational energy is available. Quantitatively, a 20% decrease of SM over the transitional climate zone of NCI can lead to a decline in ET by 10%, and a 20% increase of SM can enhance the ET by 15%.

Furthermore, by limiting the total available energy for the latent heating process, SM dominantly controls the surface energy partitioning at the land surface²⁰. A 20% decrease of SM over the NCI leads to contribute more radiational energy for sensible heating process by limiting the energy used for LHF (Fig. 10). An

increase in long-term mean SHF over the strong SM-T coupling region generally takes place due to more amount of energy consumed for heating the atmosphere through enhanced dry and warm land surface conditions¹³. Thus, drier SM conditions induce warmer atmospheric conditions over the strong SM-T coupled regions. Whereas, WET-SM experiment results indicate a relatively colder near-surface atmosphere due to entertainment of less amount of SHF through surface energy partitioning (Fig. 10). Wet SM perturbations appear to favour cloudy conditions and enhancement of atmospheric water content thereby limiting the solar radiation reaching to the Earth surface^{32,33} (also see Supplementary Figs. 1 & 2). As a consequence, the near-surface

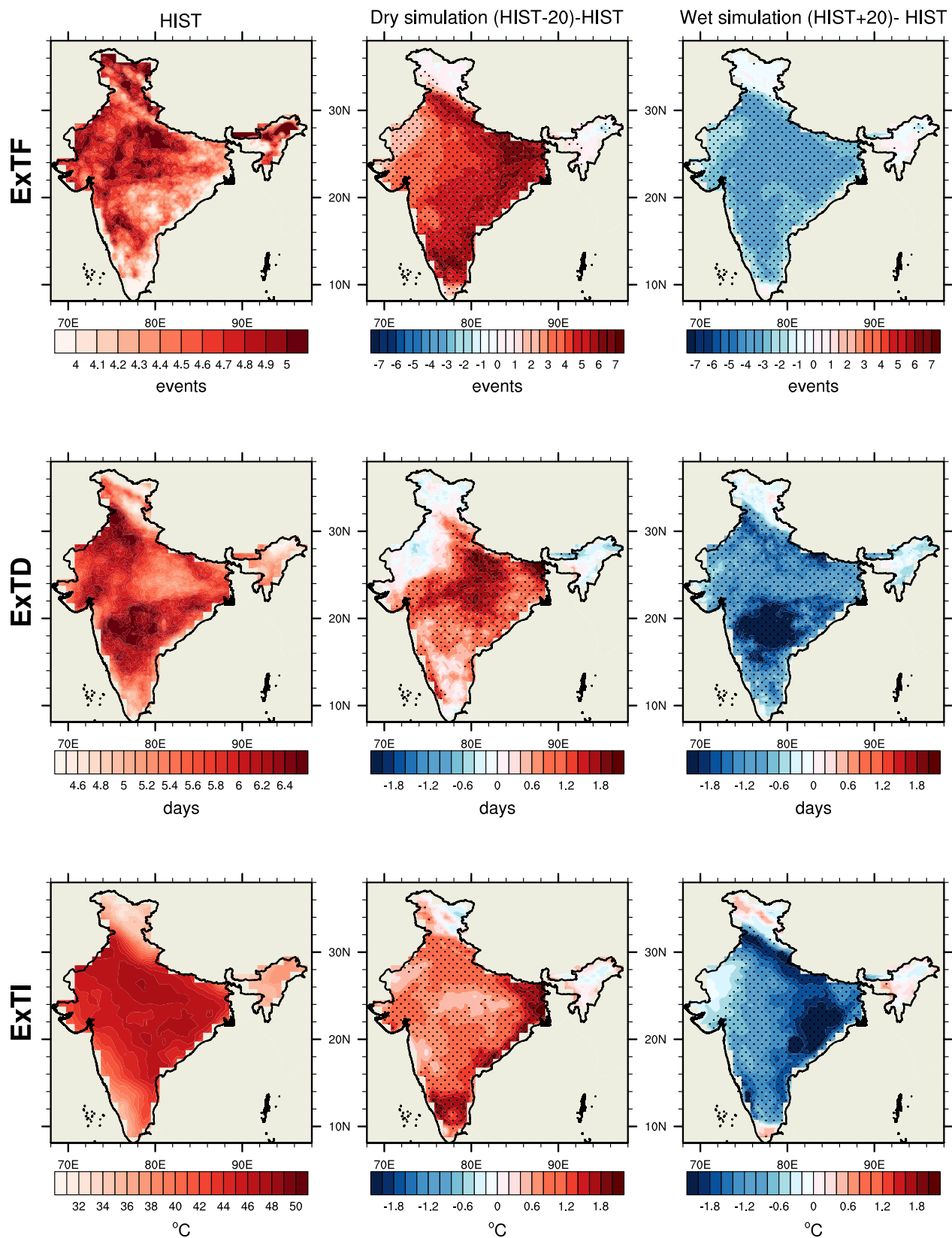


Fig. 5 Impact of SM on ExT for the historical period (1951–2010). Time-mean spatial maps of ExTF (1st row), ExTD (2nd row) and ExTI (3rd row) from the HIST experiment (1st column), difference between the HIST-20 and HIST experiments (2nd column), and difference between the HIST + 20 and HIST experiments (3rd column) during the historical period (1951–2010). Stippling in Figures indicate the regions where difference between the HIST-20/HIST + 20 and HIST experiment is significant at 95% confidence level.

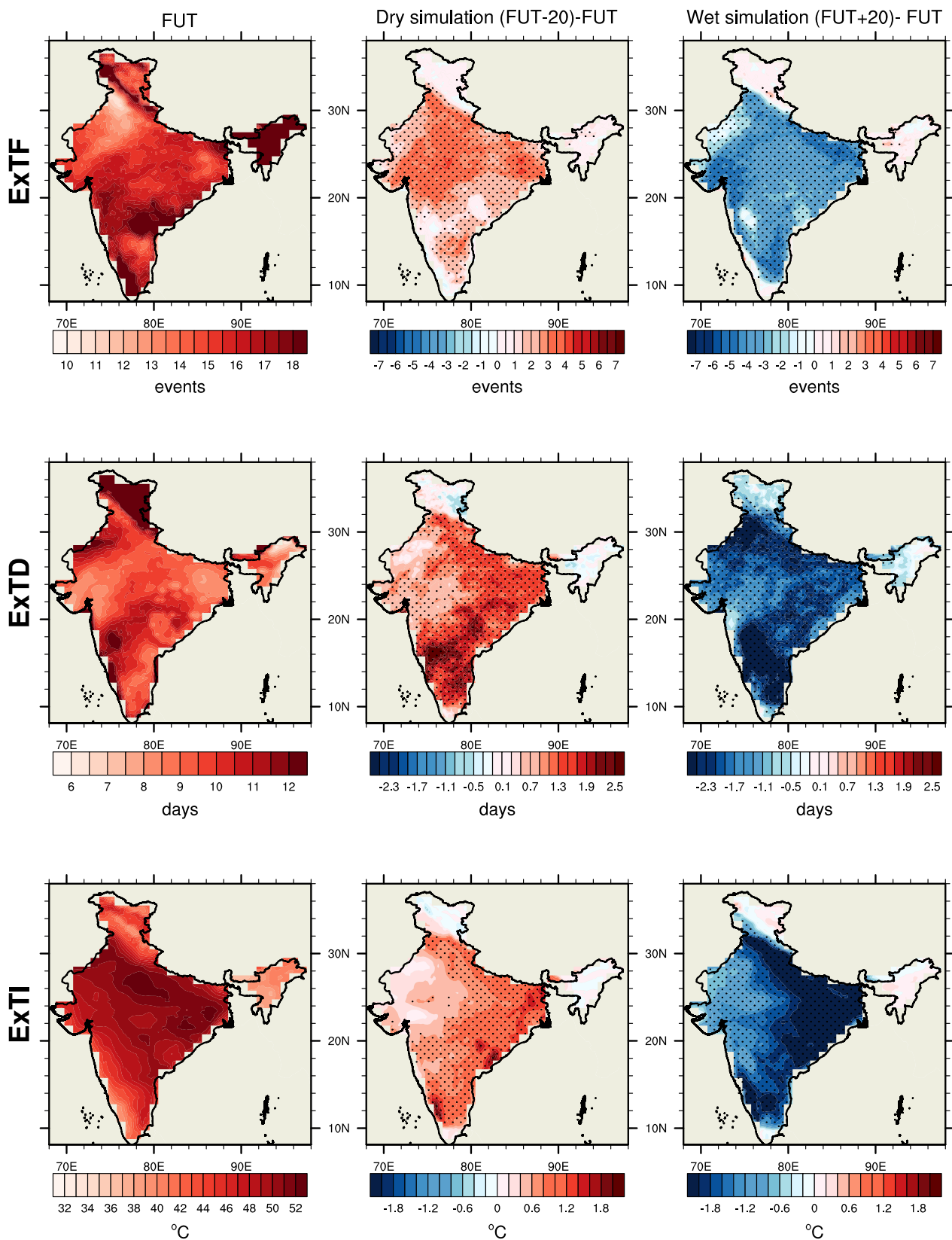


Fig. 6 Impact of SM on ExT for the future projection (2051–2100). Time-mean spatial maps of ExTF (1st row), ExTD (2nd row) and ExTI (3rd row) from the FUT experiment (1st column), difference between the FUT-20 and FUT experiments (2nd column), and the difference between FUT + 20 and FUT experiment (3rd column) during the future climate (2051–2100). Stippling in Figures indicate the regions where difference between the FUT-20/FUT + 20 and FUT experiment is significant at 95% confidence level.

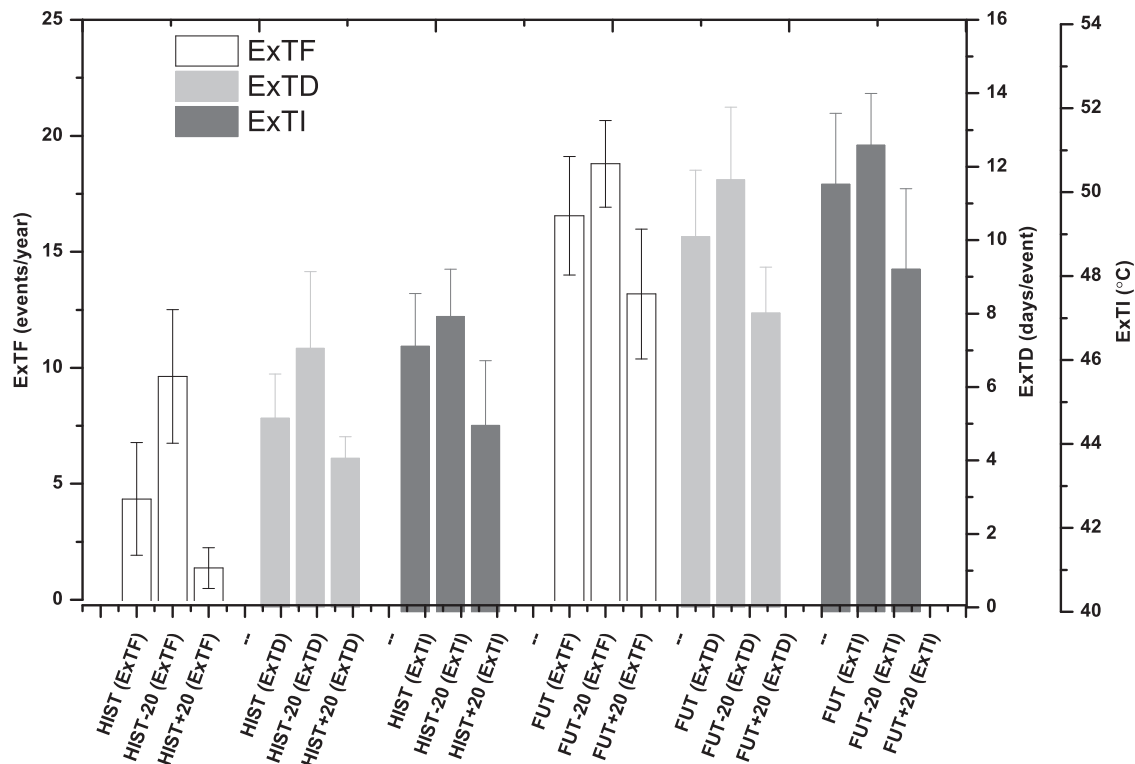


Fig. 7 Impact of SM on ExT over the NCI. Histogram compares the mean of ExTF (white), ExTD (light grey) and ExTI (dark grey) for six experiments i.e. HIST, HIST-20, HIST + 20, FUT, FUT-20 and FUT + 20, averaged over the NCI (75°E-87°E, 16°N-26°N, land only). Error bars in Figures indicate the standard deviation value of ExTF, ExTD and ExTI.

temperature remains below the normal conditions, and extreme temperature occurrence gradually subsides.

We further highlighted the sensitivity of SMM to the wet (HIST + 20) and dry (HIST-20) SM perturbations to understand the processes involved in the SM-T interactions over the Indian region. The model diagnosis suggests that the SMM time-scale over the Indian region varies from one to eight weeks (Supplementary Fig. 7). The HIST experiment shows the lowest SMM time-scale (<2 weeks) over drier regions of central as well as north-west India, whereas highest SMM (>5 weeks) found over the north and the north-east India. Furthermore, it is seen that SMM over the hotspot of strong SM-T coupling (NCI) is about 3–4 weeks. A study by Delworth and Manabe³⁹ linked the SMM time-scale with the persistence of atmospheric variability and, thus, consequently on near-surface temperature. In comparison to the wet and dry SM regions, moderate SM zones are expected to experience faster evaporative damping of SM anomalies due to available radiational energy and so have the potential to influence near-surface temperature variability. We noted a decrease in SMM across the Indian region in the HIST-20 experiment w.r.t the HIST experiment (Fig. 10). It is seen that SMM over the weak coupling regions may not be significantly modified by a 20% decrease in SM due to lower sensitivity. On the other hand, SMM time-scale behaviour is highly non-linear in the wet SM experiment over the Indian region (Fig. 10). Over the NCI, a 20% decrease of SM (HIST-20) leads to reduce SMM by 1 week, and a 20% increase of SM (HIST + 20) leads to intensify SMM by a few days (<1 week). Decrease in SMM significantly favours enhancement of SHF and warming near to the land surface, thereby reducing the ET across the hotspot of strong SM-T coupling (NCI). It is to be noted that further investigation needs to be carried out to understand the factors responsible for non-linear behaviour between SMM and WET-SM over the weak coupling zone.

DISCUSSION

The present study investigated the impact of soil moisture (SM) perturbations on the characteristics of temperature extremes (ExT) over India based on SM sensitivity experiments using the model MRI-AGCM3.2 for the historical period (1951–2010, HIST) and future (2051–2100, FUT) under the 4 K warming scenario. Our findings show that more than 70% area of the Indian landmass has experienced significant changes in the characteristics of ExT due to SM perturbations. In particular, it is noted that SM perturbations exert substantial control on the near-surface temperature variability over north-central India (NCI), a hotspot for soil moisture-temperature (SM-T) coupling, by altering the surface energy partitioning between sensible and latent heat fluxes, and soil moisture memory.

Our findings suggest that a 20% increase of SM perturbation applied on the HIST and FUT experiments, tends to decrease the frequency and duration of ExT events over NCI by nearly 60–70% and 20–30%, respectively. Conversely, a 20% decrease of SM perturbation applied on the HIST and FUT experiments, tends to increase the frequency and duration of ExT events over NCI by nearly 60–100% and 15–40%, respectively. In other words, it turns out that the impact of SM perturbations on the frequency and duration of ExT events over NCI becomes less prominent in the future (FUT) 4 K warming scenario as compared to the historical (HIST) climate. We note that this reduced impact of SM perturbations on ExT in FUT, as compared to HIST, is related to the increase of PR and SM over the Indian region which causes a decrease in the temperature difference between the surface and near-surface atmosphere (i.e. 2 m air temperature), decrease of Bowen ratio and decrease of sensible heat flux from the surface to the atmosphere (Supplementary Fig. 14).

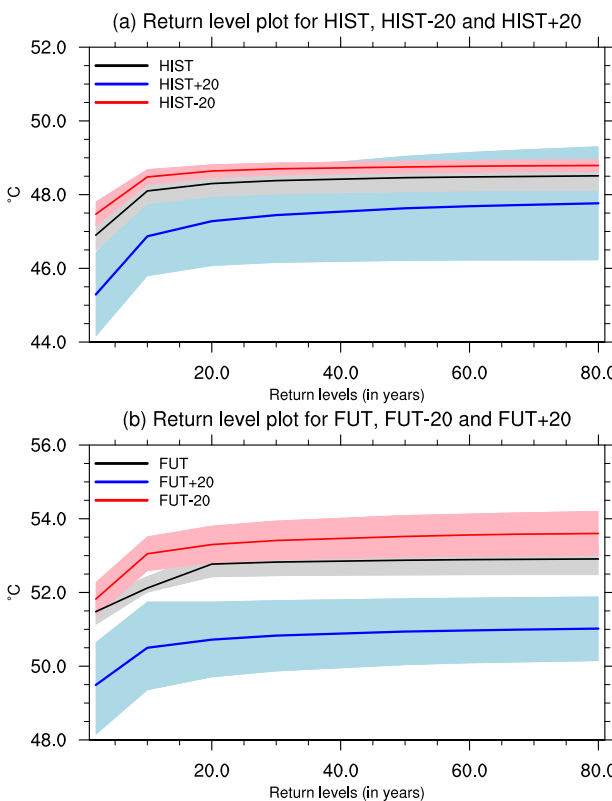


Fig. 8 Generalized extreme value (GEV) distribution. Return level plot of ExT for control run (black line), dry SM perturbation experiments (red line) and wet SM perturbation experiments (blue line) over the NCI estimated using the non-stationary GEV model fit for (a) historical period (1951–2010) and (b) future projection (2051–2100). The area between the upper and lower confidence interval of return levels for control, dry SM and wet SM experiments are filled with light grey, light red and light pink colours, respectively.

METHODS

Model and experimental setups

The revised version of the atmospheric general circulation model by the Meteorological Research Institute (MRI-AGCM3.2³⁵) from its predecessor, MRI-AGCM3.1⁴⁰, is used in the present diagnostic study for analyzing ExT and land-atmosphere interactions over India. Here, we use the ~60 km resolution version of the MRI-AGCM3.2, having 64 vertical levels and 3 active soil layers. The land component of MRI-AGCM3.2 is the Simple Biosphere model (SiB)⁴¹. The model uses observed monthly sea-surface temperature and sea ice concentration from Centennial Observation-based estimation (COBE-SST2)⁴². Whereas, climatological monthly sea ice thickness is prescribed lower boundary conditions⁴³. In addition, the external forcing is configured with observed values of global mean concentration of greenhouse gases, MRI Chemistry climate model (MRI-CCM⁴⁴) output for three-dimensional distribution of ozone, and MRI Coupled Atmosphere-Ocean General Circulation Model (MRI-CGCM3⁴⁵) output. A brief description of the MRI-AGCM3.2 model is given in the Supplementary material.

In the present study, we have evaluated six long-term simulations from high-resolution version of the MRI-AGCM3.2³⁵ (listed in Supplementary Table 1): (1) historical run (HIST: 1951–2010), (2) historical-20%SM (HIST-20: 1951–2010), (3) historical+20%SM (HIST+20: 1951–2100), (4) future 4 K projection (FUT: 2051–2100), (5) future-20%SM (FUT-20: 2051–2100), and (6) future+20%SM (FUT+20: 2051–2100). The experimental setup of the HIST and FUT simulations is same as those of d4PDF⁵. The HIST experiment use both natural (e.g. volcanoes and solar variability)

and anthropogenic forcing (e.g. greenhouse gases (GHG), aerosols etc.), whereas in FUT experiment the global mean temperature becomes 4 K warmer than the pre-industrial climate. The global increase in temperature for the future 4 K simulations corresponds to that around the end of the 21st century under Representative Concentration Pathway 8.5 scenario of CMIP5³⁵.

In addition to the HIST and FUT simulations, we have performed the wet and dry SM sensitivity experiments (HIST-20, HIST+20, FUT-20 and FUT+20) for each of two long-term simulations (HIST and FUT) to evaluate the role of SM on ExT over the Indian region. The simulations are initialized on the 1st day of each month by perturbing SM from the top three layers (upto 1–2 m depth, depending on the vegetation types⁴¹) with corresponding fields from the HIST and FUT simulations. The dry SM simulations are initialized by decreasing the SM by 20%, whereas, in the wet SM experiment, SM is increased by 20%. After introducing the initial SM perturbation, the model is subsequently integrated for one month at a time so as to generate simulations of atmospheric and land surface variables (including SM) on a month-by-month basis. The dry and wet SM sensitivity experiments were initialized with the same initial lateral boundary conditions as that of HIST and FUT simulations except for the above-mentioned SM perturbation. The control experiments (HIST and FUT) for MRI-AGCM3.2 are available for download from d4PDF database (http://search.diasjp.net/en/dataset/d4PDF_GCM). However, sensitivity experiments have been conducted specifically for this study and can be made available on request (to IITM and MRI). The impact of SM on ExT is quantified by analyzing the wet and dry SM experiments. Indeed, the impact of SM on ExT in wet and dry SM simulations is mainly modulated by altering the water as well as the energy cycle. The comparison results of SM perturbations with the control simulations are indicating a favourable condition for PR during the wet SM experiments as a consequence of an increase in cloud cover and ET, in opposite to the dry SM experiment (Supplementary Figs. 1 and 2). Furthermore, a detailed mechanism of land-atmosphere coupling processes during all the experiments is discussed in Results section.

Other data products

With a focus on understanding ExT and land-atmosphere interaction processes, we have evaluated the model simulations using observational and data assimilated products over the Indian region. Observational data include mean temperature, maximum temperature and precipitation data prepared by the India Meteorological Department (https://www.imdpune.gov.in/Clim_Pred_LRF_New/Grided_Data_Download.html)^{46,47}. Two data assimilated products are also used in the present study: (1) Global Land Data Assimilation System (GLDAS), and (2) Land Data Assimilation System (LDAS), to evaluate the model outputs. The GLDAS data is used here to examine ET, and surface energy fluxes (SHF and LHF) over the Indian region⁴⁸. Previous research has shown that GLDAS outputs are in good agreement with observations over the Indian region^{13,28,49}. Furthermore, the high resolution (~4 km) data generated by using LDAS (version 3.4.1) is explored here to validate and remove the bias in the SM over the Indian region⁵⁰. More details of the LDAS high-resolution SM data product can be found in Nayak et al.⁵⁰.

Soil moisture-temperature (SM-T) coupling

Determining the SM-T coupling is an important factor for assessing the impact of SM on ExT³¹. Based on the model experiments and analytical techniques, several methods have been proposed earlier to evaluate the coupling strength between SM and surface temperature^{27,51,52}. In the present study, quantification of surface temperature sensitivity to the SM change (SM-T coupling strength) has been carried out using the method suggested by Dirmeyer³⁸. Here, we have used a similar method for

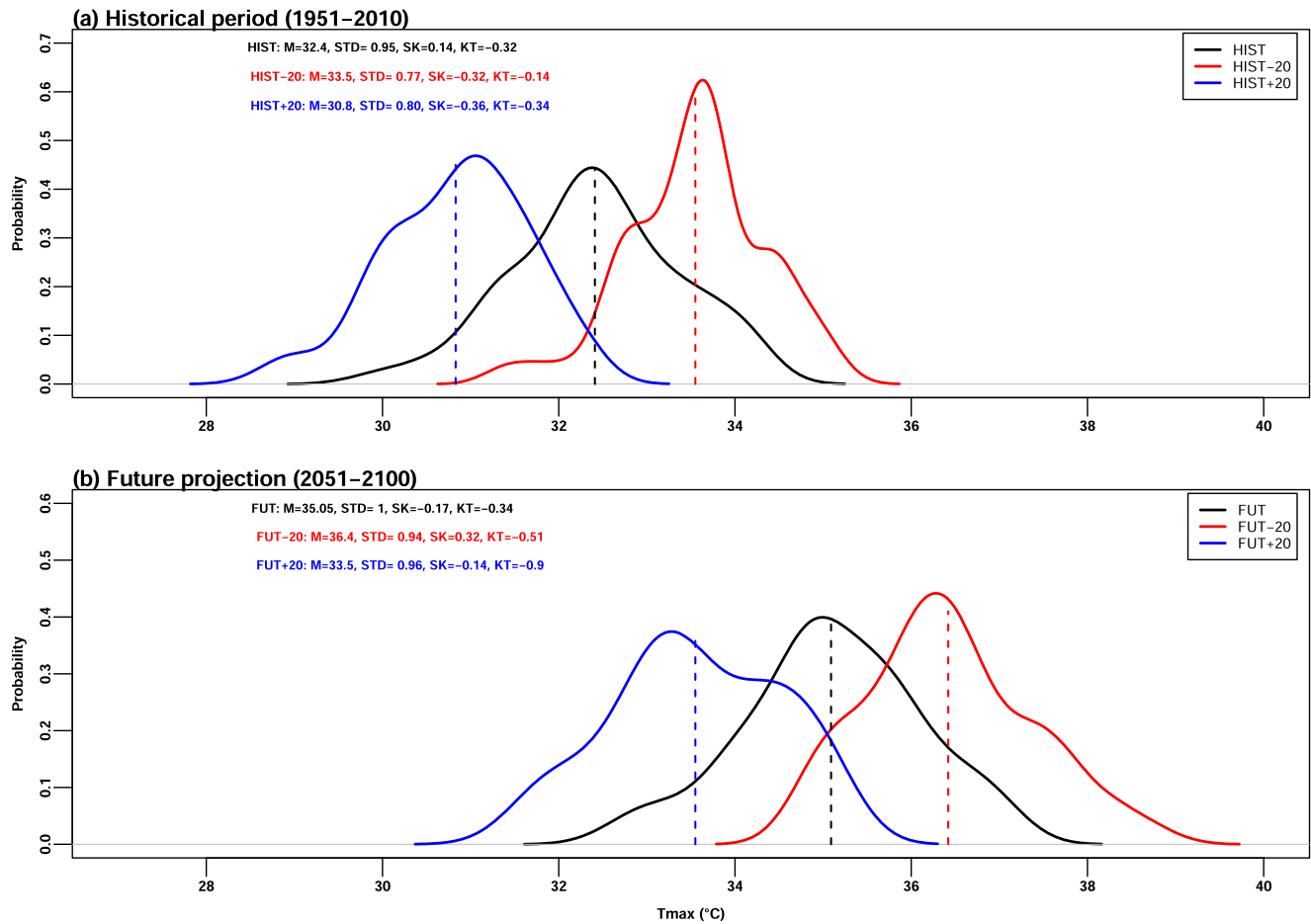


Fig. 9 Probability density function with first four moments of dispersion. Probability density function of T_{\max} over the NCI for control (black line), dry SM (red line) and wet SM (blue line) experiments during the (a) historical period (1951–2010) and (b) future projection (2051–2100). The vertical dotted line in each PDF indicates corresponding mean value. The values of the first four moments of dispersion (M mean, STD standard deviation, SK skewness, KT kurtosis) are given at the top left corners in Figure.

surface temperature sensitivity instead of using the surface energy fluxes. The method described by Dirmeyer³⁸ overcomes the shortcomings in correlation method by considering the variance of SM at each grid point. SM-T coupling metric used in this study is given in Eq. 1. In this method, we first estimate the linear regression slope (R_c) of temperature anomaly on the SM anomaly. Furthermore, the coupling metric is determined by multiplying the negative value of SM standard deviation (σ_{SM}) to regression slope (R_c).

$$\text{Coupling strength } (\Omega) = -R_c * \sigma_{SM} \quad (1)$$

Whereas, R_c denotes the slope of linear regression of temperature anomaly on SM anomaly and σ_{SM} indicates the standard deviation of SM at each grid point.

Extreme temperature indices

ExT conditions can be detected using various criteria depending upon the different climate zones⁵³. The most common definitions of ExT mainly depend on the daily maximum temperature values. The present study uses three different indices based on the daily T_{\max} from the MRI-AGCM3.2 model for evaluating ExT characteristics over India. The indices used here are similar to the standard ExT indices as referred in ETCCDI⁵⁴. Moreover, considering severity of ExT beyond the pre-monsoon season, the present study evaluates ExT characteristics on an annual scale¹³. For the historical period, extreme temperature event is defined if the daily T_{\max} value at each grid point is greater than 90th percentile

T_{\max} of the corresponding day and persists at least for three consecutive days. For the FUT experiment, we use the same definition for detecting ExT as discussed above, with 90th percentile threshold from the HIST experiment. Furthermore, total number of extreme temperature events per year is defined as extreme temperature frequency (ExTF) index, and the total number of days in each event is counted as extreme temperature duration (ExTD) index. The third index, i.e. extreme temperature intensity (ExTI), is the measure of maximum T_{\max} for each year at each grid point.

Generalized extreme value (GEV) distribution

A quantitative description of the impact of SM on ExT is given here based on the statistical approach of GEV theory²⁹. Block maxima perspective is used here to fit GEV to the model simulated yearly maximum temperature (ExTI) at each grid point, with and without considering SM as a covariate. The GEV fit performed in this study is obtained from the extReMe software package of R-programming^{55,56}. The GEV analysis is carried out in two important steps. The first step consists of stationary GEV fit for block maxima of each year without covariate (Eq. 2), whereas the second step consists of a non-stationary GEV model fit to ExTI with inclusion of SM as a covariate (Eq. 3). The GEV analysis is dependent upon three important parameters: (1) scale parameter (σ), (2) location parameter (μ), and (3) shape parameter (ξ). Scale parameter (σ) explains the variability in the dataset, mean of the fitted distribution is represented in terms of location parameter (μ)

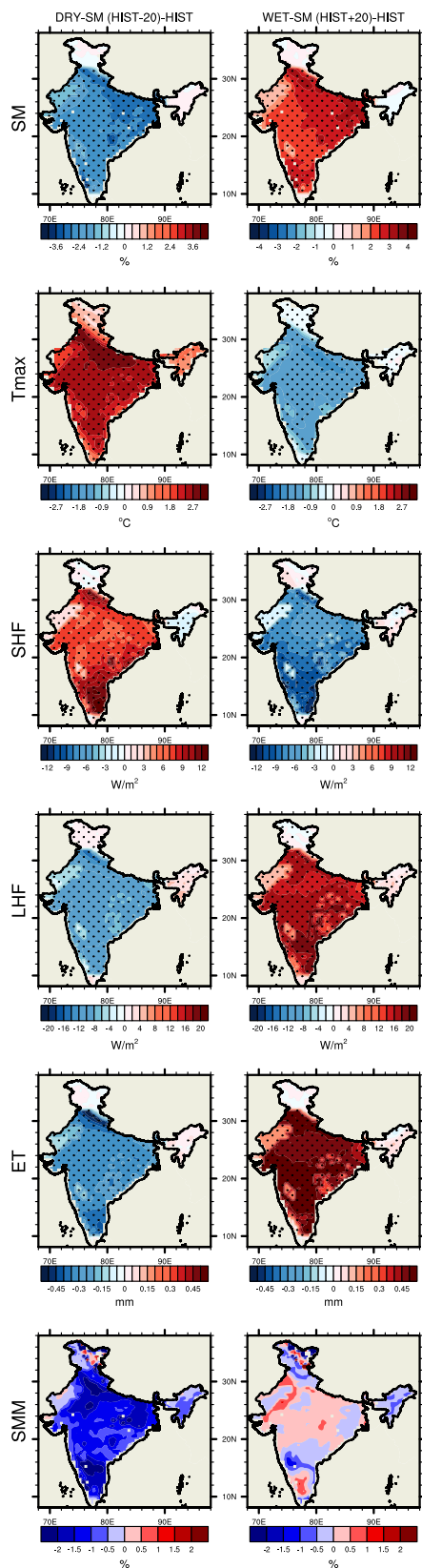


Fig. 10 Response of land-atmosphere interactions to SM perturbations. Time-mean spatial maps of difference between SM (1st row), T_{max} (2nd row), SHF (3rd row), LHF (4th row), ET (5th row) and SMM (6th row) from the HIST-20 and HIST experiments (1st column) as well as the HIST + 20 and HIST (2nd column) experiments. Stippling in Figures indicate the regions where difference between the HIST-20/HIST + 20 and HIST experiments is significant at 95% confidence level.

hotspot of strong land-atmosphere coupling (NCI).

$$G(x) = \exp\left[-\left(1 + \frac{\xi(x - \mu)}{\sigma}\right)\right] \quad (2)$$

$$\mu(y) = A_0 + A_1 y \quad (3)$$

where y is the standardized annual mean SM and fitting constants for location parameters are denoted as A_0 and A_1 .

The negative value of the estimated shape parameter for the HIST, HIST-20, HIST + 20, FUT, FUT-20 and FUT + 20 experiments indicates that ExTl follows the Weibull distribution (Supplementary Tables 2 & 4). The significance for perfect stationary and non-stationary GEV fit using the likelihood-ratio-test (LRT) shows a good fit for ExTl distribution, and the inclusion of SM as covariate improves the model fit (Supplementary Tables 2, 3, 4 & 5). In the GEV analysis, impact of SM on extremes is demonstrated by analyzing the differences between 50-year return levels of ExTl from dry and wet SM sensitivity experiments for the historical and the future climate.

Soil moisture memory (SMM)

The property of the soil to remember wet or dry anomalies caused by atmospheric forcing is generally termed as SMM^{22,25}. The present study measures the SMM in terms of time-scale lag at which the autocorrelation drops to 1/e (e-folding time-scale) of its value¹³. The method of e-folding time-scale is based on the 30-day lag autocorrelation values of SM anomalies considering the exponential decay of the SM autocorrelation function (Eq. 4).

$$r(\tau) = e^{-\tau/\lambda} \quad (4)$$

where $r(\tau)$ is the autocorrelation function, τ is the lag and λ is called the decay time-scale. SMM analysis is also extended to the wet SM and dry SM experiments to explore the impact of SMM on ExTl.

In this study, statistical significance of difference between two different experiments is analyzed through the *t*-test⁵⁷. In addition to this, we have also estimated the trend and the Pearson correlation coefficient^{57,58}.

DATA AVAILABILITY

The control experiments (i.e. HIST and FUT simulations) from MRI-AGCM3.2 are free to download from d4PDF database http://search.diasjp.net/en/dataset/d4PDF_GCM and http://search.diasjp.net/en/dataset/d4PDF_RCM. Outputs of SM sensitivity experiments can be made available on request (to MRI and IITM) for research purposes. Temperature (minimum and maximum) and rainfall gridded data is available at IMD database https://imdpune.gov.in/Clim_Pred_LRF_New/Grided_Data_Download.html. Other datasets such as GLDAS is freely available to download from <http://disc.gsfc.nasa.gov/hydrology>, whereas, LDAS can be obtained from IMD with appropriate permissions.

CODE AVAILABILITY

Model runs and codes to produce the figures are available from the corresponding author with proper request.

Received: 4 May 2022; Accepted: 8 February 2023;
Published online: 21 February 2023

and the shape of the fitted distribution is shape parameter (ξ) (i.e. Gumbel: $\xi = 0$, Frechet: $\xi > 0$, Weibull: $\xi < 0$). The GEV analysis is carried out on the area-averaged value of ExTl and SM over the

REFERENCES

- Perkins, S. E., Alexander, L. V. & Nairn, J. R. Increasing frequency, intensity and duration of observed global heatwaves and warm spells. *Geophys. Res. Lett.* **39**, 1–5 (2012).
- Perkins-Kirkpatrick, S. E. & Lewis, S. C. Increasing trends in regional heatwaves. *Nat. Commun.* **11**, 1–8 (2020).
- Satyanarayana, G. C. & Rao, D. V. B. Phenology of heat waves over India. *Atmos. Res.* **245**, 105078 (2020).
- Das, J. & Umamahesh, N. V. Heat wave magnitude over India under changing climate: projections from CMIP5 and CMIP6 experiments. *Int. J. Climatol.* 1–21 <https://doi.org/10.1002/joc.7246>. (2021).
- Mizuta, R. et al. Over 5,000 years of ensemble future climate simulations by 60-km global and 20-km regional atmospheric models. *Bull. Am. Meteorol. Soc.* **98**, 1383–1398 (2017).
- Murari, K. K., Ghosh, S., Patwardhan, A., Daly, E. & Salvi, K. Intensification of future severe heat waves in India and their effect on heat stress and mortality. *Reg. Environ. Chang.* **15**, 569–579 (2015).
- Krishnan, R. et al. Assessment of climate change over the Indian region. assessment of climate change over the Indian region: a report of the ministry of earth sciences (MoES) (government of India 2020). https://doi.org/10.1007/978-981-15-4327-2_5.
- Singh, B. B., Singh, M. & Singh, D. An overview of climate change over South Asia: observations, projections, and recent advances. in *Practices in regional science and sustainable regional development* 263–267 (Springer, 2021). https://doi.org/10.1007/978-981-16-2221-2_12.
- De, U. S., Dube, R. K. & Rao, G. S. P. Extreme weather events over India in the last 100 years. *J. Indian Geophys. Union* **9**, 173–187 (2005).
- Kothawale, D. R., Revadekar, J. V. & Kumar, K. R. Recent trends in pre-monsoon daily temperature extremes over India. *J. Earth Syst. Sci.* **119**, 51–65 (2010).
- Raghavan, K. A climatological study of severe heat waves in India. *Indian J. Meteorol. Geophys.* **17**, 581–586 (1966).
- Dimri, A. P. Comparison of regional and seasonal changes and trends in daily surface temperature extremes over India and its subregions. *Theor. Appl. Climatol.* **136**, 265–286 (2019).
- Ganeshi, N. G., Mujumdar, M., Krishnan, R. & Goswami, M. Understanding the linkage between soil moisture variability and temperature extremes over the Indian region. *J. Hydrol.* **589**, 125183 (2020).
- Im, E. S., Pal, J. S. & Eltahir, E. A. B. Deadly heat waves projected in the densely populated agricultural regions of South Asia. *Sci. Adv.* **3**, 1–7 (2017).
- Patz, J. A., Campbell-Lendrum, D., Holloway, T. & Foley, J. A. Impact of regional climate change on human health. *Nature* **438**, 310–317 (2005).
- Ratnam, J. V., Behera, S. K., Ratna, S. B., Rajeevan, M. & Yamagata, T. Anatomy of Indian heatwaves. *Sci. Rep.* **6**, 1–11 (2016).
- Rohini, P., Rajeevan, M. & Srivastava, A. K. On the variability and increasing trends of heat waves over India. *Sci. Rep.* **6**, 1–9 (2016).
- De, U. S. & Mukhopadhyay, R. K. Severe heat wave over the Indian subcontinent in 1998, in perspective of global climate. *Curr. Sci.* **75**, 1308–1311 (1998).
- Joshi, M. K., Rai, A., Kulkarni, A. & Kucharski, F. Assessing changes in characteristics of hot extremes over India in a warming environment and their driving mechanisms. *Sci. Rep.* **10**, 1–14 (2020).
- Seneviratne, S. I. et al. Investigating soil moisture-climate interactions in a changing climate: a review. *Earth Sci. Rev.* **99**, 125–161 (2010).
- Yuan, G. et al. Understanding the partitioning of the available energy over the semi-arid areas of the Loess Plateau, China. *Atmosphere (Basel)* **8**, 87–93 (2017).
- Delworth, T. L. & Manabe, S. The influence of potential evaporation on the variabilities of simulated soil wetness and climate. *J. Clim.* **1**, 523–547 (1988).
- Entin, J. K. et al. Temporal and spatial scales of observed soil moisture variations in the extratropics. *J. Geophys. Res.* **105**, 11865–11877 (2000).
- Koster, R. D. & Suarez, M. J. Soil moisture memory in climate models. *J. Hydrometeorol.* **2**, 558–570 (2001).
- Wu, W. & Dickinson, R. E. Time scales of layered soil moisture memory in the context of land-atmosphere interaction. *J. Clim.* **17**, 2752–2764 (2004).
- Manabe, S. & Delworth, T. The temporal variability of soil wetness and its impact on climate. <https://doi.org/10.1007/BF00134656>. (1990).
- Miralles, D. G., Van Den Berg, M. J., Teuling, A. J. & De Jeu, R. A. M. Soil moisture-temperature coupling: a multiscale observational analysis. *Geophys. Res. Lett.* **39**, 2–7 (2012).
- Mujumdar, M. et al. A study of field-scale soil moisture variability using the cosmic-ray soil moisture observing system (COSMOS) at IITM Pune site. *J. Hydrol.* **597**, 126102 (2021).
- Whan, K. et al. Impact of soil moisture on extreme maximum temperatures in Europe. *Weather Clim. Extrem.* **9**, 57–67 (2015).
- Erdenebat, E. & Sato, T. Role of soil moisture-atmosphere feedback during high temperature events in 2002 over Northeast Eurasia. *Prog. Earth Planet. Sci.* **5**, 37 (2018).
- Seneviratne, S. I., Lüthi, D., Litschi, M. & Schär, C. Land-atmosphere coupling and climate change in Europe. *Nature* **443**, 205–209 (2006).
- Asharaf, S., Dobler, A. & Ahrens, B. Soil moisture-precipitation feedback processes in the Indian summer monsoon season. *J. Hydrometeorol.* **13**, 1461–1474 (2012).
- Raman, S., Mohanty, U. C., Reddy, N. C., Alapaty, K. & Madala, R. V. Numerical simulation of the sensitivity of summer monsoon circulation and rainfall over India to land surface processes. *Pure Appl. Geophys.* **152**, 781–809 (1998).
- Shukla, J. & Mintz, Y. Influence of land-surface evapotranspiration on the earth's climate. *Sci. (80-)* **215**, 1498–1501 (1982).
- Mizuta, R. et al. Climate simulations using MRI-AGCM3.2 with 20-km grid. *J. Meteorol. Soc. Jpn.* **90**, 233–258 (2012).
- Soriani, E., Mediero, L. & Garijo, C. Selection of bias correction methods to assess the impact of climate change on flood frequency curves. *Water (Switzerland)* **11**, 2266–2267 (2019).
- Taylor, K. E. Summarizing multiple aspects of model performance in a single diagram. *J. Geophys. Res.* **106**, 7183–7192 (2001).
- Dirmeyer, P. A. The terrestrial segment of soil moisture-climate coupling. *Geophys. Res. Lett.* **38**, 1–5 (2011).
- Delworth, T. & Manabe, S. Climate variability and land-surface processes. *Adv. Water Resour.* **16**, 3–20 (1993).
- Kitoh, A., Ose, T., Kurihara, K., Kusunoki, S. & Sugi, M. Projection of changes in future weather extremes using super-high-resolution global and regional atmospheric models in the KAKUSHIN program: results of preliminary experiments. *Hydrol. Res. Lett.* **3**, 49–53 (2009).
- Hirai, M. et al. Validation of a new land surface model operational global model using the CEOP observation dataset The CEOP (Coordinated Enhanced Observing (JMA-GSM) using CEOP Appendix. *J. Meteorol. Soc. Japan* **85A**, 1–24 (2007).
- Hirahara, S., Ishii, M. & Fukuda, Y. Centennial-scale sea surface temperature analysis and its uncertainty. *J. Clim.* **27**, 57–75 (2014).
- Bourke, R. H. & Garret, R. P. Sea ice thickness distribution in the Arctic Ocean. *Cold Reg. Sci. Technol. Elsevier Sci. Publ. B. V.* **13**, 259–280 (1987).
- Deushi, M. & Shibata, K. Development of a meteorological research institute chemistry-climate model version 2 for the study of tropospheric and stratospheric chemistry. *Pap. Meteorol. Geophys.* **62**, 1–46 (2011).
- Yukimoto, S. et al. A new global climate model of the Meteorological Research Institute: MRI-CGCM3: -Model description and basic performance-. *J. Meteorol. Soc. Jpn.* **90**, 23–64 (2012).
- Srivastava, Rajeevan, M. & Kshirsagar, S. R. Development of a high resolution daily gridded temperature data set (1969–2005) for the Indian region. *Atmos. Sci. Lett.* **10**, 249–254 (2009).
- Pai, D. S., Sridhar, L., Badwaik, M. R. & Rajeevan, M. Analysis of the daily rainfall events over India using a new long period (1901–2010) high resolution ($0.25^\circ \times 0.25^\circ$) gridded rainfall data set. *Clim. Dyn.* **45**, 755–776 (2015).
- Rodell, B. M. et al. The global land data assimilation system. *Bull. Am. Meteorol. Soc.* **85**, 381–394 (2004).
- Sathyamadhi, A., Karipot, A., Ranalkar, M. & Prabhakaran, T. Evaluation of soil moisture data products over Indian region and analysis of spatio-temporal characteristics with respect to monsoon rainfall. *J. Hydrol.* **542**, 47–62 (2016).
- Nayak, H. P. et al. High-resolution gridded soil moisture and soil temperature datasets for the Indian monsoon region. *Sci. Data* **5**, 1–17 (2018).
- Dong, J. & Crow, W. T. Use of satellite soil moisture to diagnose climate model representations of European soil moisture-air temperature coupling strength. *Geophys. Res. Lett.* **45**, 12,884–12,891 (2018).
- Seneviratne, S. I. et al. Impact of soil moisture-climate feedbacks on CMIP5 projections: first results from the GLACE-CMIP5 experiment. *Geophys. Res. Lett.* **40**, 5212–5217 (2013).
- Nairn, J. & Fawcett, R. *Defining heatwaves: heatwave defined as a heat-impact event servicing all community and business sectors in Australia*. CAWCR technical report. 551.5250994 (2013).
- Roy, S. Spatial patterns of trends in seasonal extreme temperatures in India during 1980–2010. *Weather Clim. Extrem.* **24**, 100203 (2019).
- Core Team, R. A language and environment for statistical computing. R foundation for statistical computing, Vienna, Austria (2016). Available at: <https://www.r-project.org/>.
- Gilleland, E. & Katz, R. W. extRemes 2.0: An Extreme Value Analysis Package in R. *J. Stat. Softw.* **72**, 1–39 (2016).
- Wilks, D. S. Statistical methods in the atmospheric sciences. *J. Chem. Inf. Model.* **91**, 131–178 (Elsevier, 2011).
- Maity, R. *Statistical methods in hydrology and hydroclimatology*. 191–227 (Springer, 2018).

ACKNOWLEDGEMENTS

The authors are grateful to the Director, Indian Institute of Tropical Meteorology (IITM, India), for the support to carry out this research work. The authors would like to

thank Dr. Ryo Mizuta and Dr. Yukiko Imada (Senior Researchers at the Meteorological Research Institute) for their support on model experiments. The IITM HPC support is duly acknowledged. The IITM is fully funded by the Ministry of Earth Sciences, Government of India. This work was also supported by Sumitomo foundation and MEXT program for the advanced studies of climate change projection (SENTAN) Grant Numbers JPMXD0722680395 and JPMXD0722680734. We sincerely thank three anonymous reviewers and the Editor for their useful suggestions in improving the manuscript.

AUTHOR CONTRIBUTIONS

N.G.G. initiated and led this study. M.M., R.K., B.B.S., and T.T. conceived and supervised the study. N.G.G., M.M.G. performed the analyses and Y.T. performed model simulations. N.G.G., M.M. and B.B.S. wrote the original draft. All authors participated in discussions and contributed to review and editing the manuscript.

COMPETING INTERESTS

The authors declare no competing interests.

ADDITIONAL INFORMATION

Supplementary information The online version contains supplementary material available at <https://doi.org/10.1038/s41612-023-00334-1>.

Correspondence and requests for materials should be addressed to Milind Mujumdar.

Reprints and permission information is available at <http://www.nature.com/reprints>

Publisher's note Springer Nature remains neutral with regard to jurisdictional claims in published maps and institutional affiliations.



Open Access This article is licensed under a Creative Commons Attribution 4.0 International License, which permits use, sharing, adaptation, distribution and reproduction in any medium or format, as long as you give appropriate credit to the original author(s) and the source, provide a link to the Creative Commons license, and indicate if changes were made. The images or other third party material in this article are included in the article's Creative Commons license, unless indicated otherwise in a credit line to the material. If material is not included in the article's Creative Commons license and your intended use is not permitted by statutory regulation or exceeds the permitted use, you will need to obtain permission directly from the copyright holder. To view a copy of this license, visit <http://creativecommons.org/licenses/by/4.0/>.

© The Author(s) 2023, corrected publication 2023